Rapid atomic layer etching of Al_2O_3 using sequential exposures of hydrogen fluoride and trimethylaluminum with no purging

David R. Zywotko,[1] Jacques Faguet,[2] and Steven M. George[1,3]
[1]*Department of Chemistry and Biochemistry, University of Colorado, Boulder, Colorado 80309*
[2]*TEL Technology Center, America, LLC, Austin, Texas 78741*
[3]*Department of Mechanical Engineering, University of Colorado, Boulder, Colorado 80309*

(Received 9 June 2018; accepted 17 September 2018; published 8 October 2018)

A dramatic increase in the Al_2O_3 atomic layer etching (ALE) rate versus time was demonstrated using sequential, self-limiting exposures of hydrogen fluoride (HF) and trimethylaluminum (TMA) as the reactants with no purging. The normal purging expected to be required to prevent chemical vapor etching or chemical vapor deposition (CVD) is not necessary during the Al_2O_3 ALE. This purgeless, rapid atomic layer etching (R-ALE) was studied from 250 to 325 °C using various techniques. *In situ* quartz crystal microbalance (QCM) measurements monitored Al_2O_3 R-ALE at 300 °C. The Al_2O_3 R-ALE process produced linear etching versus number of R-ALE cycles. Each HF exposure fluorinates the Al_2O_3 substrate to produce an AlF_3 surface layer. Each subsequent dose of TMA then undergoes a ligand-exchange transmetalation reaction with the AlF_3 surface layer to yield volatile products. Using reactant partial pressures of HF = 320 mTorr and TMA = 160 mTorr, the fluorination and ligand-exchange reactions produced a mass change per cycle (MCPC) of −32.1 ng/(cm^2 cycle) using sequential, 1 s exposures for both HF and TMA with no purging. This MCPC equates to a thickness loss of 0.99 Å/cycle or 0.49 Å/s. Comparison experiments using the same reactant exposures and purge times of 30 s yielded nearly identical MCPC values. These results indicate that the etch rates for Al_2O_3 R-ALE are much faster than for normal Al_2O_3 ALE because of shorter cycle times with no purging. Smaller MCPC values were also observed at lower reactant pressures for both Al_2O_3 R-ALE and Al_2O_3 ALE. The QCM studies showed that the Al_2O_3 R-ALE process was self-limiting versus reactant exposure. *Ex situ* spectroscopic ellipsometry and x-ray reflectivity (XRR) measurements revealed temperature-dependent etch rates from 0.02 Å/cycle at 270 °C to 1.12 Å/cycle at 325 °C. At lower temperatures, AlF_3 growth was the dominant mechanism and led to an AlF_3 atomic layer deposition (ALD) growth rate of 0.33 Å/cycle at 250 °C. The transition temperature between AlF_3 growth and Al_2O_3 etching occurred at ~270 °C. XRR scans showed that the Al_2O_3 ALD films were smoothed by Al_2O_3 R-ALE at temperatures ≥270 °C. Additionally, patterned wafers were used to compare Al_2O_3 R-ALE and normal Al_2O_3 ALE in high aspect ratio structures. Scanning electron microscope images revealed that the etching was uniform for both processes and yielded comparable etch rates per cycle in the high aspect ratio structures and on flat wafers. The HF and TMA precursors were also intentionally overlapped to explore the behavior when both precursors were present at the same time. Similar to ALD, where precursor overlap produces CVD, precursor overlap during Al_2O_3 ALE leads to AlF_3 CVD. However, any AlF_3 CVD growth that occurs during precursor overlap is removed by spontaneous AlF_3 etching during the subsequent TMA exposure. This spontaneous AlF_3 etching explains why no purging is necessary during R-ALE. R-ALE represents an important advancement in the field of thermal ALE by producing rapid etching speeds that will facilitate many ALE applications. *Published by the AVS.* https://doi.org/10.1116/1.5043488

I. INTRODUCTION

Atomic layer etching (ALE) can yield Ångstrom-level control of thin film removal based on sequential, self-limiting surface reactions.[1] ALE is the reverse of atomic layer deposition (ALD).[2] ALE is usually defined using a surface activation reaction where the surface is first modified by the adsorption of reactive species such as chlorine or fluorine.[1,3] During "plasma ALE," this activated surface layer can then be removed by high-energy collisions from energetic ions or noble gas atoms.[1] Plasma ALE has been employed to etch a variety of substrates including Si,[4,5] Ge,[6] GaAs,[7] SiO_2,[8] HfO_2,[9] and graphite.[10] During "thermal ALE," the activated surface layer can be removed by a thermal surface reaction that produces stable, volatile reaction products. Thermal ALE has been utilized to etch many materials including Al_2O_3,[11–15] AlF_3,[16] HfO_2,[17] SiO_2,[18] ZnO,[19] AlN,[20] TiN,[21] and W.[22]

Thermal ALE has many similarities to ALD.[23] Both thermal ALE and ALD can be performed with gas phase precursors without the need of nonthermal enhancement. The reliance only on gas phase precursors enables both thermal ALE and ALD to etch or deposit isotropically and conformally on substrates. ALD requires a purge step between the sequential reactant exposures to prevent precursor overlap that would produce chemical vapor deposition (CVD).[24] The purge times during ALD are typically much longer than the reactant

exposure times.[24,25] In thermal ALE, purge times are also assumed to be necessary to prevent chemical vapor etching (CVE) or CVD. However, no studies have been performed to test this assumption.

The need for the purge time in thermal ALE may be different because ALD and thermal ALE can usually be performed with the same two reactants. For example, AlF_3 ALD and Al_2O_3 ALE can both be achieved using trimethylaluminum (TMA) and hydrogen fluoride (HF).[11,13,26] Under the same reactant pressures and exposures, low temperatures will produce AlF_3 ALD and higher temperatures will produce Al_2O_3 ALE.[11,13,26] Higher or lower reactant pressures may also favor AlF_3 ALD or Al_2O_3 ALE, respectively. The competition between ALD and thermal ALE may also affect the purge times during thermal ALE. For example, if AlF_3 CVD occurs during TMA and HF precursor overlap, then the TMA exposure after precursor overlap may spontaneously etch the AlF_3 CVD film and eliminate the need for a purge time during thermal Al_2O_3 ALE using TMA and HF.[26]

ALE cycle times without purging could be very short. Compared with the purge times required during typical ALD processing, purgeless ALE cycle times could easily be ≥10 times shorter than typical ALD cycle times. To test these ideas, this study explored thermal Al_2O_3 ALE using sequential exposures of HF and TMA with no purging.[13] This new form of purgeless thermal ALE is defined as rapid atomic layer etching (R-ALE). Al_2O_3 R-ALE was examined using sequential, 1 s exposures for both HF and TMA with no purge times. Etch rates were compared with the etch rates obtained using purge times. The self-limiting nature of the reactions during R-ALE was also explored to define the R-ALE process.

Experiments also examined the competition between Al_2O_3 R-ALE and AlF_3 ALD versus temperature under the same reaction conditions. The transition temperature between etching or growth was compared with the decrease or increase in surface roughness. Additional experiments also intentionally overlapped the HF and TMA exposures and quantified the etching behavior versus precursor overlap time. These investigations help to establish a framework for understanding R-ALE and the usefulness of R-ALE for various applications.

II. EXPERIMENT

A. Reactants and pulse sequences

The Al_2O_3 R-ALE was performed using HF and TMA as the reactants.[13] The HF source was an HF-pyridine solution (70 wt. % HF, Sigma-Aldrich). At room temperature, this liquid HF source provides 90–100 Torr of HF vapor pressure above the solution with negligible pyridine vapor pressure.[17,26] The HF-pyridine solution was transferred to a gold-plated bubbler under an N_2 atmosphere and subjected to three freeze-pump-thaw degassing cycles. The TMA (97%, Sigma-Aldrich) and HF-pyridine were held at room temperature during the Al_2O_3 R-ALE.

The experiments were conducted using a t_1, t_2, t_3, t_4 reactant pulse timing sequence. During the timing sequence, the values of t_1 and t_3 denote the precursor pulse times while t_2 and t_4 are the start times for the precursor pulses relative to the end of the previous precursor pulse. All times were in seconds. In this work, a purgeless reactant pulse timing sequence was utilized that can be expressed as (1, 0, 1, 0). This timing sequence is defined by a 1 s pulse of precursor A, immediately followed by a 1 s pulse of precursor B with no purge time. This pulse sequence is illustrated in Fig. 1(a).

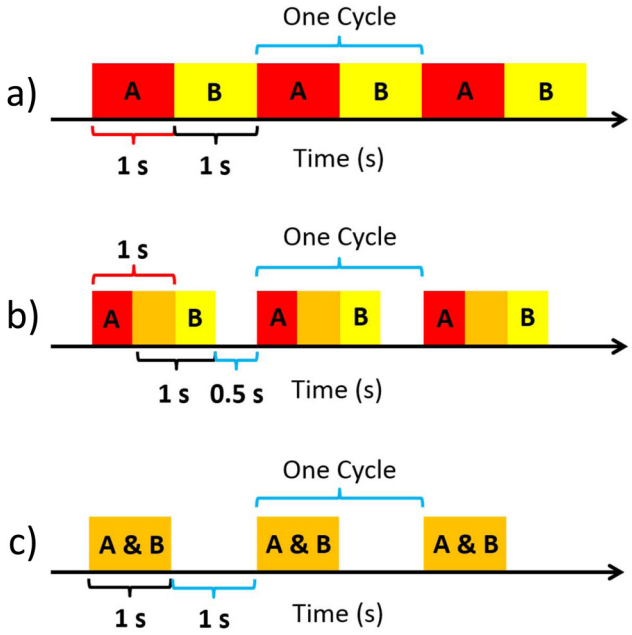

FIG. 1. Experimental pulse timing sequences with 1 s precursor exposures and total cycle time of 2 s: (a) timing sequence of (1, 0, 1, 0) with no purging; (b) timing sequence of (1, −0.5, 1, 0.5) with a pulse overlap of 0.5 and 0.5 s purge; (c) timing sequence of (1, −1, 1, 1) with a pulse overlap of 1 and 1 s purge.

An overlap of precursor exposures was also utilized to explore CVE or possible CVD. In these experiments, negative time values are used in the dose timing sequence. For example, the timing sequence of (1, −0.5, 1, 0.5) indicates that a 1 s pulse of HF begins and, after 0.5 s, a 1 s pulse of TMA begins. This gives 0.5 s of precursor overlap. When the 1 s TMA pulse comes to an end, a 0.5 s purge brings the total cycle time to 2 s. This pulse sequence is shown in Fig. 1(b). In another example, complete overlap of two 1 s exposures of HF and TMA with a 1 s purge after the concurrent HF and TMA exposures is illustrated in Fig. 1(c). This pulse timing sequence can be expressed as (1, −1, 1, 1).

Most of the Al_2O_3 R-ALE experiments were performed at 300 °C.[13] Controlled R-ALE was achieved by sequential exposures of HF and TMA. Computer-controlled pneumatic dose valves coupled with metering valves ensured consistent precursor exposures during each etching cycle. The metering valves limited the HF and TMA pressure transients to 320 and 160 mTorr, respectively, for most of the experiments. During the experiments that demonstrated self-limiting etching behavior, the reactant partial pressures were adjusted using the metering valves. Additional Al_2O_3 R-ALE experiments were performed versus temperature from 250 to 325 °C under similar conditions.

B. Reactor and *in situ* quartz crystal microbalance

A hot-walled stainless steel reaction chamber was used to perform the ALE and ALD processes.[25] The reaction chamber was pumped by a chemical series dual-stage rotary vane pump (Pascal 2010C1, Pfeiffer). A bakeable capacitance manometer (Baratron 121A, MKS) monitored the process pressure during the experiments. The pump maintained a base pressure of ~20 mTorr without any N_2 gas flowing through the reactor.

An *in situ* quartz crystal microbalance (QCM) was positioned inside the isothermal reaction zone in the reactor.[25] The QCM was used to monitor mass changes while pulsing the precursors during the ALE and ALD reactions. The *in situ* QCM system consisted of a sensor housing (modified CDS-A0E47, Inficon) equipped with a quartz sensor crystal (gold coated, 6 MHz, 285 °C optimized, Inficon). The QCM measurements were recorded by a thin film deposition monitor (Maxtek TM-400, Inficon) with a mass resolution of ~0.375 ng/cm^2. A low-outgassing, high temperature epoxy (Epo-Tek H21D, Epoxy Technology Inc.) sealed the unit to prevent backside deposition and corrosion of the internal electrical components.

The reactor temperature was held constant to ±0.1 °C by a proportional-integral-derivative temperature controller (2408, Eurotherm) and power controller (7100A, Eurotherm). These devices controlled two insulating ceramic fiber heaters (VS102A06S and VS102A12S, Watlow) that encased the reactor body. A preheat zone raised the precursor and carrier gases to the reaction temperature prior to reaching the QCM. Thermal equilibration of process gases to the reaction temperature is critical to prevent erroneous mass recordings.[27] Additionally, an equilibration time of 4 h was allowed following changes to the temperature set-point. The uniform isothermal environment is important for obtaining high quality, low-noise QCM measurements.

During experimental operation, three mass flow controllers delivered a constant flow of 190 sccm of ultrahigh purity (UHP) N_2 gas (99.999%, Airgas) into the reactor. The reactants were housed in separate lines upstream of the reaction chamber. Each line had a dedicated mass flow controller (Type 1179A, MKS) that streamed 85 sccm of N_2 gas. This flow served as a precursor carrier gas and purged the line prior to entering the main reactor chamber. An additional mass flow controller (Type 1159B, MKS) provided a steady 20 sccm of N_2 gas through the QCM sensor housing and purged the backside of the QCM sensor before exiting downstream of the active sensor area. The QCM was allowed to equilibrate for 10 min following changes to the reactor background pressure.[28] The total N_2 gas flow maintained a base pressure of ~1.5 Torr. Experimental pressures during the optimized R-ALE process varied with reactant exposure around ~1.95 Torr.

Prior to mounting the QCM system in the reactor, a film of ~100 nm of Al_2O_3 was deposited in the reactor using Al_2O_3 ALD to prevent HF from corroding the stainless steel reactor walls. Once installed, Al_2O_3 ALD substrate films were also grown on the QCM crystal using TMA (97%, Sigma-Aldrich) and H_2O (high-performance liquid chromatography grade, submicron filtered, Fisher Scientific) at 300 °C prior to each etching experiment. The TMA was contained in a metal cylinder (Sure/Pac, Sigma-Aldrich) and the H_2O was housed in a glass bubbler. Witness coupons of Si(100) confirmed normal Al_2O_3 ALD growth at 1.01 Å/cycle, consistent with previous reports at 300 °C.[29,30]

C. *Ex situ* analysis using x-ray reflectivity, spectroscopic ellipsometry, and x-ray photoelectron spectroscopy

Coupons measuring 2 cm × 2 cm were prepared from 125 mm boron-doped Si wafers (*p*-type, <100>, Silicon Valley Microelectronics) for Al_2O_3 deposition and Al_2O_3 etching. The coupons were cleaned with deionized water, acetone, and methanol and then blown dry with UHP N_2 and immediately inserted into the reactor. The samples were allowed to equilibrate for 2 h prior to the Al_2O_3 ALD. Al_2O_3 ALD films were grown on the coupons using 500 cycles of Al_2O_3 ALD with TMA and H_2O at 300 °C. The coated samples were then unloaded and the Al_2O_3 film thickness was determined by *ex situ* spectroscopic ellipsometry (SE). Subsequently, the samples were rinsed with methanol and dried with N_2 prior to reinsertion into the reactor for the R-ALE experiments. Al_2O_3 R-ALE experiments were conducted between 250 and 325 °C.

A high resolution grazing-incidence x-ray diffractometer (Bede D1, Jordan Valley Semiconductors) performed x-ray reflectivity (XRR) scans of the Al_2O_3 films before and after Al_2O_3 R-ALE. These XRR measurements employed Cu Kα radiation at $\lambda = 1.540$ Å. The x-ray tube utilized a filament voltage of 40 kV and a current of 35 mA. Using a 15 arc sec step size, XRR scans were recorded from 300 to 6000 arc sec with a 5 s acquisition time. The scans were fit using BEDE REFS analysis software (Jordan Valley Semiconductors) to determine film thickness, film density, and surface roughness.

Ex situ SE was performed using a spectroscopic ellipsometer (M-2000UI, J.A. Woollam Co.) to determine the film thickness after the ALD and R-ALE processes. SE data were collected between $\lambda = 245$ nm and $\lambda = 1690$ nm at an angle of 70°. The SE data were analyzed using the CompleteEASE software provided by J.A. Woollam Co. This software fits the amplitude ratio (ψ) and phase difference (Δ) based on a custom model to determine the film thickness. The accuracy of the model was confirmed by comparison with selected XRR thickness measurements.

X-ray photoelectron spectroscopy (XPS) measurements were conducted to determine the film composition. Surface survey scans were performed by an x-ray photoelectron spectrometer (PHI 5600) using monochromatic Al Kα radiation ($E = 1486$ eV). The data were collected by AugerScan (RBD Instruments) and analyzed using CasaXPS software (Casa Software Ltd.).

D. Patterned wafers for scanning electron microscopy analysis

Patterned Si wafer samples containing high aspect ratio structures were received from Tokyo Electron Ltd. The surface of these samples contained an SiO_2 film with a

thickness of ~24 nm. The samples were loaded as received into the reactor. An Al_2O_3 ALD film with a thickness of ~28 nm was then deposited using sequential TMA and H_2O exposures at 300 °C. After measurement of the Al_2O_3 ALD film thickness, the samples were reloaded into the reactor for Al_2O_3 etching. The Al_2O_3 ALE and R-ALE processes were conducted with HF and TMA pressures of 320 and 160 mTorr, respectively. The Al_2O_3 ALE and R-ALE processes were performed for 130 cycles. The background N_2 pressure was ~1.2 Torr. Purge times ranging from 30 to 0 s provided a comparison between ALE and R-ALE, respectively, in high aspect ratio structures.

The Al_2O_3 film thicknesses after Al_2O_3 ALD, Al_2O_3 ALE, and Al_2O_3 R-ALE were determined using *ex situ* scanning electron microscopy (SEM) performed at the TEL Technology Center, America, LLC in Albany, NY. SEM images were obtained using an accelerating voltage of 5 kV and a probe current of 2 μA. The magnification level was 200 000×.

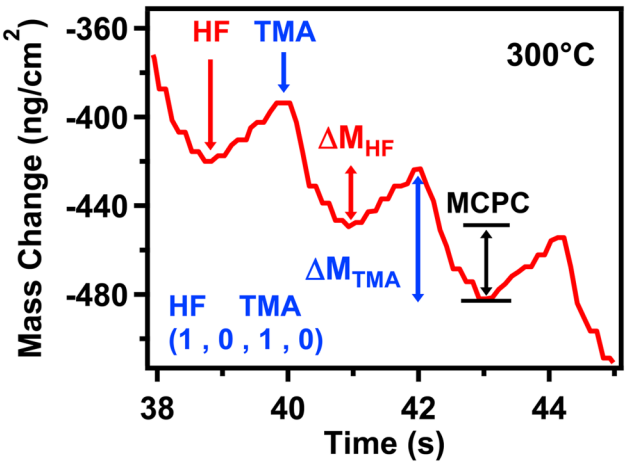

FIG. 3. Expanded segment of Fig. 2 showing the mass changes during individual HF and TMA exposures at 300 °C with the timing sequence of (1, 0, 1, 0).

III. RESULTS AND DISCUSSION

A. Quartz crystal microbalance studies

One R-ALE reaction cycle consisted of a 1 s dose of HF immediately followed by a 1 s dose of TMA without any purging. This timing sequence is designated as (1, 0, 1, 0) and is illustrated in Fig. 1(a). Figure 2 shows the QCM measurements of mass change versus time during 50 cycles of Al_2O_3 R-ALE using partial pressures of HF = 320 mTorr and TMA = 160 mTorr at 300 °C. The result is rapid linear etching of the Al_2O_3 film with an average mass change per cycle (MCPC) of −32.1 ng/(cm^2 cycle). This MCPC represents the removal of 1.9×10^{14} Al_2O_3 units/(cm^2 cycle). This MCPC corresponds to an etch rate of 0.99 Å/cycle using an Al_2O_3 ALD film density of 3.25 g/cm^3 obtained from XRR measurements.

Figure 3 shows an expanded region of the QCM results presented in Fig. 2 for three cycles of HF and TMA exposures at 300 °C. The arrows indicate the start of the HF and TMA exposures. The mass changes during the individual exposures of HF and TMA are denoted by ΔM_{HF} and ΔM_{TMA}, respectively. The mass changes for all the individual precursor pulses are very distinct despite the absence of a purge time. The total MCPC is defined as $MCPC = \Delta M_{HF} + \Delta M_{TMA}$.

Figure 4 shows a summary of values for ΔM_{HF}, ΔM_{TMA}, and MCPC versus cycle number for the 50 R-ALE cycles in Fig. 2. The mass changes during the HF and TMA exposures are constant throughout the 50 R-ALE cycles at $\Delta M_{HF} = 28.6$ ng/(cm^2 cycle) and $\Delta M_{TMA} = -60.7$ ng/(cm^2 cycle). These mass changes lead to an overall MCPC = −32.1 ng/(cm^2 cycle). Each 1 s HF exposure results in a mass gain as the Al_2O_3 substrate is fluorinated to form an AlF_3 surface layer. The fluorination reaction is given by $Al_2O_3(s) + 6HF(g) \rightarrow 2AlF_3(s) + 3H_2O(g)$.[12–14] This reaction is favorable with $\Delta G = -49.1$ kcal/mol at 300 °C.[31] Subsequent exposures of TMA cause a mass loss as volatile $AlF(CH_3)_2$ products are formed through the ligand-exchange reaction $AlF_3(s) + 2Al(CH_3)_3(g) \rightarrow 3AlF(CH_3)_2(g)$.[13]

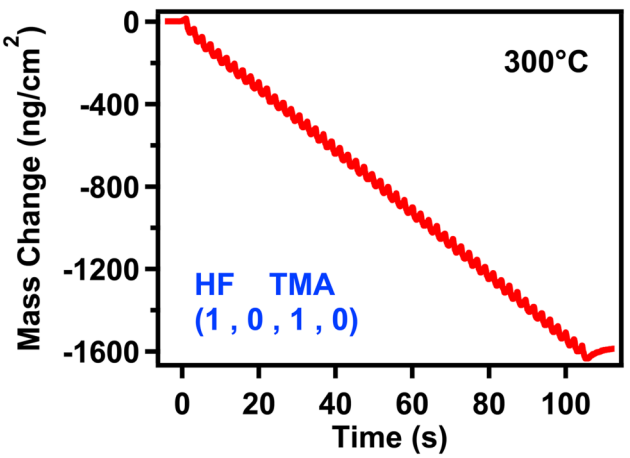

FIG. 2. Mass change vs time for Al_2O_3 R-ALE using sequential exposures of HF and TMA at 300 °C for 50 cycles with a timing sequence of (1, 0, 1, 0). The reactant pressures were HF = 320 mTorr and TMA = 160 mTorr.

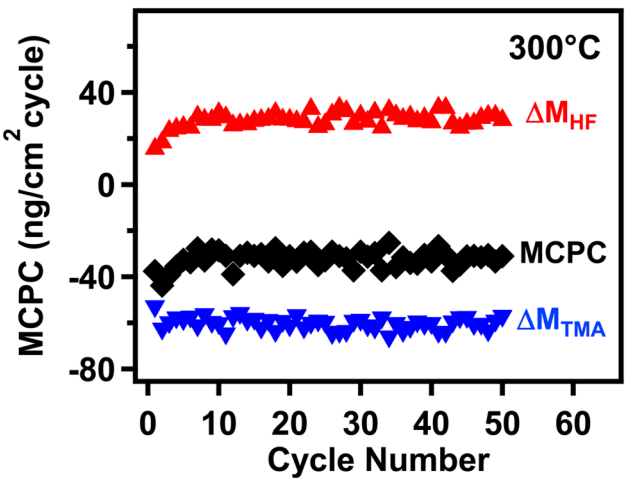

FIG. 4. Mass change after each HF exposure (ΔM_{HF}), mass change after each TMA exposure (ΔM_{TMA}), and total MCPC vs number of R-ALE cycles at 80 °C.

The R-ALE process was examined for self-limiting behavior by comparing the MCPC as a function of partial pressure for each reactant using the timing sequence of (1, 0, 1, 0). The results are summarized in Fig. 5. During these experiments, the pressure of one precursor was varied while the pressure of the second precursor was held constant. The exposure time for both precursors was 1 s.

In Fig. 5(a), the partial pressure of HF is varied from 0 to 640 mTorr while the partial pressure of the TMA exposure is fixed at 160 mTorr. With increasing HF pressure, the MCPC steadily drops and levels off at −32.1 ng/(cm^2 cycle) with HF pressures ≥320 mTorr. The MCPC decreases as larger HF pressures yield a thicker fluorination layer that can then be removed by the TMA ligand-exchange reaction. However, the fluoride layer eventually reaches a self-limiting thickness at the higher HF pressures.

Figure 5(b) analyzes the self-limiting behavior of the TMA pressure during Al_2O_3 R-ALE. The HF partial pressure was held at 320 mTorr while the TMA partial pressure was varied from 0 to 320 mTorr. The MCPC decreases with increasing TMA pressure and reaches a plateau at −32.1 ng/(cm^2 cycle) with a TMA pressure of 160 mTorr. This limit is defined by the finite thickness of the initial fluoride layer that can be removed by the TMA ligand-exchange reaction.

The fluorination reaction is limited because the fluoride layer acts as a diffusion barrier for additional fluorination. Similar behavior is observed for silicon oxidation as described by Deal-Grove kinetics.[32] In addition, the fluorination of Al_2O_3 to AlF_3 introduces compressive stress in the AlF_3 layer. The mass increase for the fluorination reaction is $\Delta M_{HF} = 28.6$ ng/(cm^2 cycle). This mass increase is consistent with 2.610×10^{14} Al_2O_3 units/cm^2 converted to 5.220×10^{14} AlF_3 units/cm^2 through the reaction $Al_2O_3(s) + 6HF(g) \rightarrow 2AlF_3(s) + 3H_2O(g)$. The Pilling-Bedworth ratio, R_{PB}, quantifies the molar expansion of the conversion. The Pilling-Bedworth ratio is defined by the ratio of the molar volumes of the two materials.[33] The Pilling-Bedworth ratio for 2(AlF_3 molar volume)/Al_2O_3 molar volume is $R_{PB} = 1.8$. The compressive stress in the AlF_3 layer will act to restrict further fluorination and lead to a self-limiting fluorination reaction.

The R-ALE process with no purge time generates a pressure profile that is different than the pressure profiles observed during ALD or ALE experiments with long purge times. Figure 6(a) displays the QCM mass change from Fig. 2 during 50 cycles of Al_2O_3 R-ALE at 300 °C. Figure 6(b) shows the corresponding pressure profile versus time. Without a purge, the pressure increases from the initial pressure of ~1.5 Torr defined by the N_2 gas flow to ~2.0 Torr with the addition of the pressure from the HF and TMA precursors and their reaction products. The pressure oscillates steadily around ~1.95 Torr with the sequential HF and TMA exposures. The pressure rises and falls slightly as HF and TMA are dosed into the reactor, respectively. In contrast, the pressure returns to the background pressure during the long purge times for typical ALD or ALE experiments.

The Al_2O_3 R-ALE process was compared with the earlier Al_2O_3 ALE process using HF and TMA as reactants.[13] The Al_2O_3 R-ALE process in this study used a timing

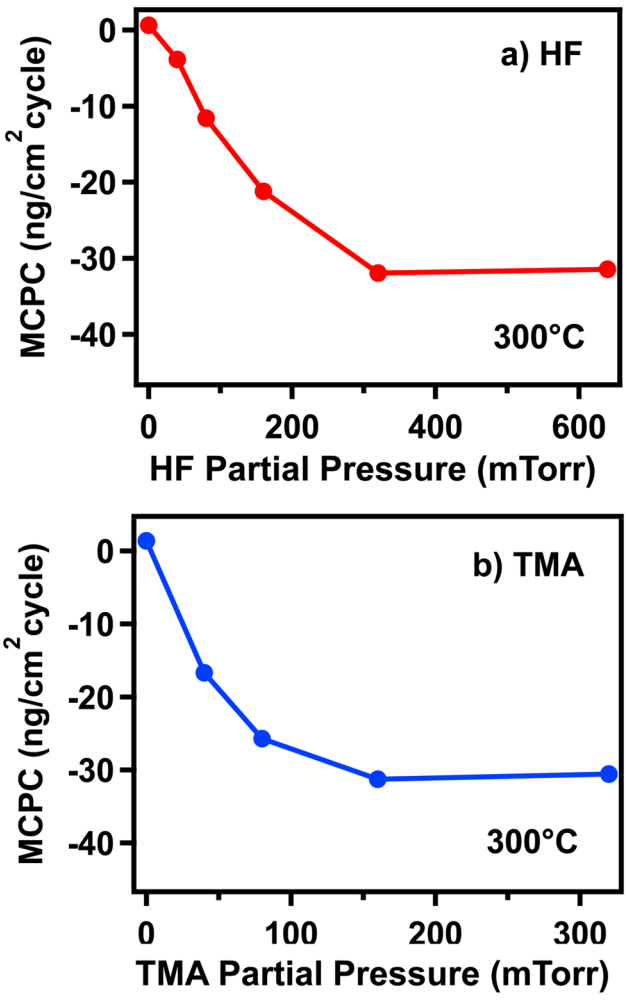

FIG. 5. MCPC at 300 °C vs precursor partial pressure for (a) HF exposure of 1 s with variable partial pressure and TMA exposure fixed at 1 s and 160 mTorr and (b) TMA exposure of 1 s with variable partial pressure and HF exposure fixed at 1 s and 320 mTorr.

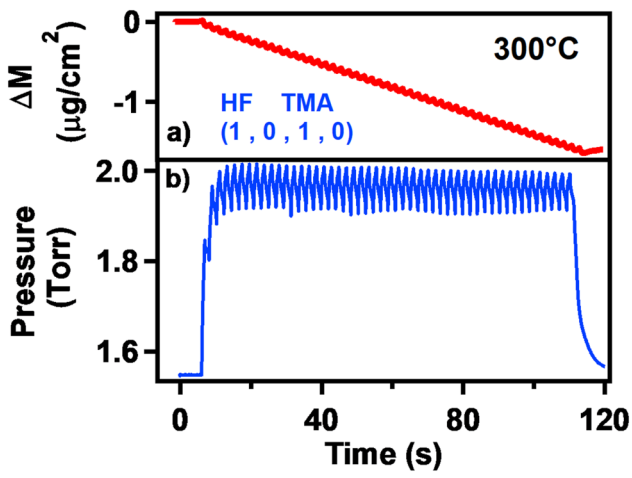

FIG. 6. (a) Mass change vs time for Al_2O_3 R-ALE using sequential exposures of HF and TMA at 300 °C for 50 cycles with a timing sequence of (1, 0, 1, 0) using pressures of HF = 320 mTorr and TMA = 160 mTorr. (b) Pressure during Al_2O_3 R-ALE for the QCM results shown in (a).

sequence of (1, 0, 1, 0) with pressures of HF = 320 mTorr and TMA = 160 mTorr, respectively. The earlier Al_2O_3 ALE process used a timing sequence of (1, 30, 2, 30) with pressures of HF = 80 mTorr and TMA = 40 mTorr, respectively.[13] To compare Al_2O_3 R-ALE and Al_2O_3 ALE with the same reactant exposures as employed in Fig. 2, Al_2O_3 ALE was performed at pressures of HF = 320 mTorr and TMA = 80 mTorr using a timing sequence of (1, 30, 2, 30).

Figure 7 shows the QCM measurements of mass change versus time for this comparison experiment. The Al_2O_3 etching is linear versus the number of ALE cycles with an average MCPC of −32.9 ng/(cm^2 cycle). This MCPC is nearly identical to the MCPC of −32.1 ng/(cm^2 cycle) obtained for Al_2O_3 R-ALE in Fig. 2. The only difference is the purge time. The Al_2O_3 R-ALE has a short cycle time of 2 s. In contrast, Al_2O_3 ALE has a much longer cycle time of 63 s. The Al_2O_3 etch rate is 36.5 times faster for Al_2O_3 R-ALE.

Al_2O_3 R-ALE was also performed at lower reactant pressures that were similar to the earlier Al_2O_3 ALE process.[13] Figure 8(a) shows the QCM measurements of mass change versus time using pressures of HF = 80 mTorr and TMA = 80 mTorr with a timing sequence of (1, 0, 1, 0). The R-ALE Al_2O_3 ALE is again linear versus number of ALE cycles with a smaller average MCPC of −14.8 ng/(cm^2 cycle). In addition, Fig. 8(b) displays QCM measurements that were conducted using the same reactant exposures as in Fig. 8(a) with a timing sequence of (1, 30, 2, 30). The reactant pressures were HF = 80 mTorr and TMA = 40 mTorr. The Al_2O_3 etching is linear versus number of ALE cycles with a nearly equivalent average MCPC of −15.7 ng/(cm^2 cycle).

These comparison experiments for Al_2O_3 R-ALE and Al_2O_3 ALE performed at the same reactant exposures indicate that the MCPCs are not affected by the purging time. The MCPCs are larger at the higher reactant pressures. However, the MCPCs are nearly identical for no purging and a purge time of 30 s. The larger MCPCs at the higher reactant pressures are believed to result from larger Al_2O_3 fluorination at higher HF pressure and larger HF exposure. Thicker AlF_3 layers from Al_2O_3 fluorination then results in more etching during the ligand-exchange reaction with TMA.

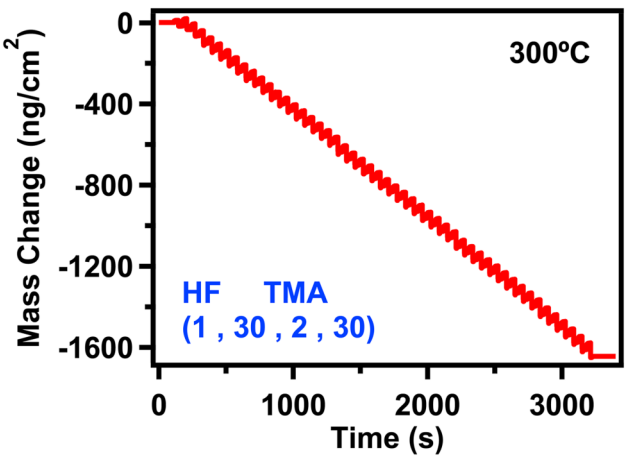

FIG. 7. Mass change vs time for Al_2O_3 ALE using sequential exposures of HF and TMA at 300 °C for 50 cycles with a timing sequence of (1, 30, 2, 30). The reactant pressures were HF = 320 mTorr and TMA = 80 mTorr.

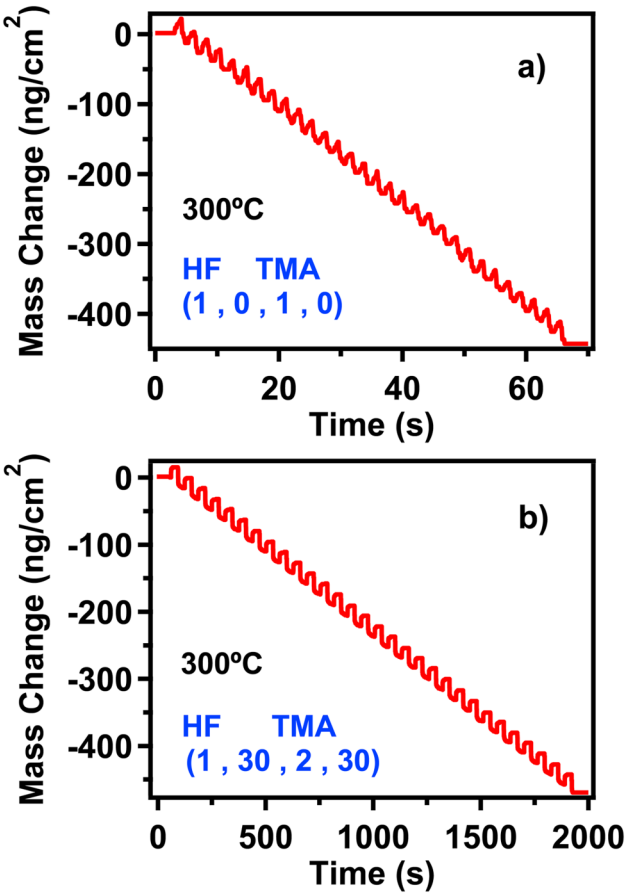

FIG. 8. (a) Mass change vs time for Al_2O_3 ALE using sequential exposures of HF and TMA at 300 °C for 30 cycles with a timing sequence of (1, 0, 1, 0). The reactant pressures were HF = 80 mTorr and TMA = 80 mTorr. (b) Mass change vs time for Al_2O_3 ALE using sequential exposures of HF and TMA at 300 °C for 30 cycles with a timing sequence of (1, 30, 2, 30). The reactant pressures were HF = 80 mTorr and TMA = 40 mTorr.

Larger Al_2O_3 etch rates were also observed at higher HF pressures by Al_2O_3 ALE at 300 °C using HF and TMA in a chamber previously passivated with LiF.[15] The Al_2O_3 etch rates increased from 0.9 to 1.4 Å/cycle as the HF pressure increased from 200 to 800 mTorr.[15] The Al_2O_3 etch rates also exceeded 3.0 Å/cycle for multiple HF exposures at a HF pressure of 500 mTorr.[15] XPS analysis confirmed that these multiple HF exposures led to higher F at. % in the Al_2O_3 films.[15]

B. Spectroscopic ellipsometry, x-ray reflectivity, and x-ray photoelectron measurements

SE and XRR measurements were employed to examine the thickness of Al_2O_3 ALD films after various numbers of Al_2O_3 R-ALE cycles at 300 °C with the timing sequence of (1, 0, 1, 0) using pressures of HF = 320 mTorr and TMA = 160 mTorr. Figure 9 shows that the Al_2O_3 thickness decreases linearly versus number of Al_2O_3 R-ALE cycles. The SE and XRR measurements are in very good agreement. The average Al_2O_3 R-ALE etch rate was 0.99 Å/cycle. This etch rate is

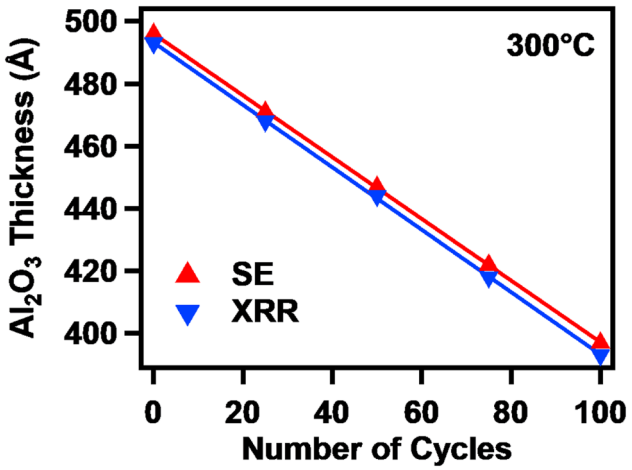

FIG. 9. Al_2O_3 thickness vs number of R-ALE cycles using sequential exposures of HF and TMA at 300 °C with a timing sequence of (1, 0, 1, 0). The reactant pressures were HF = 320 mTorr and TMA = 160 mTorr. Al_2O_3 thickness was measured using SE and XRR measurements.

in excellent agreement with the etch rate determined by the QCM studies.

Al_2O_3 R-ALE was observed to be very dependent on temperature. Figure 10 displays the thickness change versus number of R-ALE cycles for temperatures between 250 and 325 °C with a pulse sequence of (1, 0, 1, 0) using pressures of HF = 320 mTorr and TMA = 160 mTorr. The thickness change varies from +0.33 Å/cycle at 250 °C to −1.12 Å/cycle at 325 °C. The thickness change remains near zero (+0.02 Å/cycle) at 270 °C. There is competition between Al_2O_3 etching and AlF_3 growth using HF and TMA as reactants. This competition has been reported earlier using FTIR studies of Al_2O_3 etching and AlF_3 growth versus temperature.[11] The increase in film thickness at temperatures below ~270 °C is produced by AlF_3 growth. The decrease in the film thickness at temperatures above ~270 °C results from Al_2O_3 etching.[11]

Figure 11 displays the etch rate versus temperature obtained from 100 cycles of R-ALE with a pulse sequence of (1, 0, 1, 0) using pressures of HF = 320 mTorr and TMA = 160 mTorr. Below 270 °C, the etch rate is negative as AlF_3 ALD occurs during the sequential HF and TMA exposures.[11,26] Above 270 °C, the etch rate is positive and increases at higher temperatures. This increase in etch rate results from more efficient TMA ligand-exchange reactions with AlF_3 at higher temperatures.[13] The etch rate slowly levels off as the temperature approaches 325 °C. This leveling off may be attributed to the TMA removing all of the fluoride layer at higher temperatures. In addition, the thermal decomposition of the TMA precursor above 300 °C may also affect the ligand-exchange reaction.[34]

The surface coverage of adsorbed HF molecules plays a key role in the transition between AlF_3 growth and Al_2O_3 etching.[11] At temperatures below ~270 °C, adsorbed HF molecules can react with the incoming TMA exposure and form $AlF(CH_3)_2$* and $AlF_2(CH_3)$* surface species.[11,26] These species may then react with the next HF exposure resulting in AlF_3 growth. At temperatures above ~270 °C, there are less HF* surface species present and less $AlF_x(CH_3)_y$* surface intermediates will form with the incoming TMA exposure.[11] Additionally, if the $AlF_x(CH_3)_y$* surface intermediates are formed, they may desorb prior to the next HF exposure. In the absence of adsorbed $AlF_x(CH_3)_y$* surface intermediates, the incoming HF is free to fluorinate the Al_2O_3 surface. Likewise, in the absence of HF* surface species, the incoming TMA is free to undergo ligand-exchange reactions with the AlF_3 surface layer. These conditions are optimum for Al_2O_3 etching.

Figure 12(a) shows the surface roughness of Al_2O_3 ALD films as a function of the number of R-ALE cycles at 300 °C with a pulse sequence of (1, 0, 1, 0) using pressures of HF = 320 mTorr and TMA = 160 mTorr. The initial Al_2O_3 films were grown at 150 °C on Si(100) with TMA and H_2O using a timing sequence of (1, 15, 1, 15). The shorter purge times were chosen deliberately to introduce surface

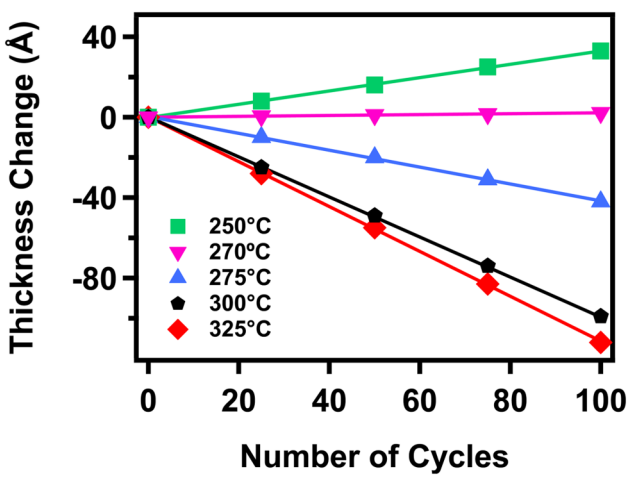

FIG. 10. Thickness change of Al_2O_3 film vs number of R-ALE cycles for various temperatures using sequential exposures of HF and TMA with a timing sequence of (1, 0, 1, 0). The reactant pressures were HF = 320 mTorr and TMA = 160 mTorr.

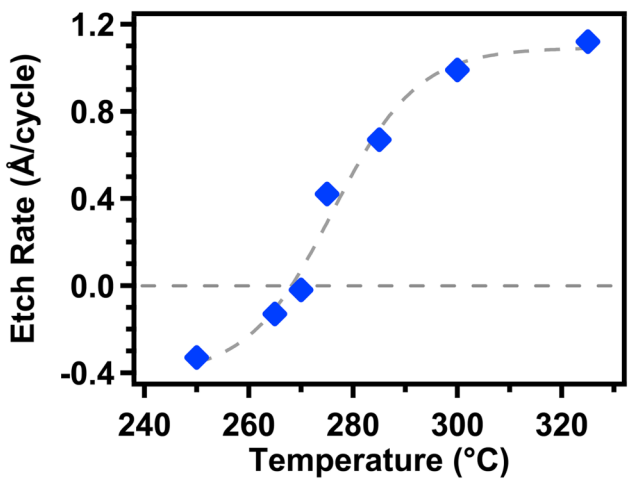

FIG. 11. Etch rate vs temperature using sequential exposures of HF and TMA with a timing sequence of (1, 0, 1, 0). The reactant pressures were HF = 320 mTorr and TMA = 160 mTorr. Negative etch rate is consistent with growth of the AlF_3 CVD film.

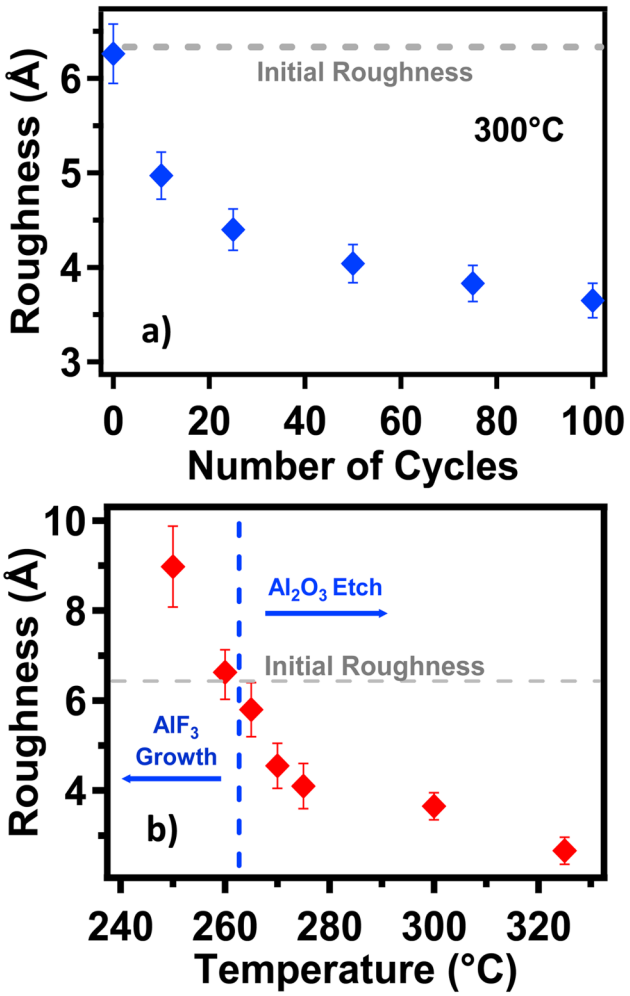

FIG. 12. (a) Roughness of the Al_2O_3 film vs number of R-ALE cycles. (b) Roughness of the Al_2O_3 film vs temperature after 100 R-ALE cycles. R-ALE was performed using sequential exposures of HF and TMA with a timing sequence of (1, 0, 1, 0) at 300 °C. The reactant pressures were HF = 320 mTorr and TMA = 160 mTorr. Initial surface roughness was 6.26 Å.

roughness. XRR scans revealed a starting Al_2O_3 surface roughness of 6.26 Å. The surface is progressively smoothed by Al_2O_3 ALE. Following 100 cycles of Al_2O_3 R-ALE, the surface roughness was reduced to 3.65 Å.

Similar surface smoothing during thermal ALE has been observed earlier during Al_2O_3 ALE,[14] ZnO ALE,[19] and HfO_2 ALE.[17] A reduction of surface roughness during thermal ALE is attributed to the conformal nature of thermal ALE. Features that deviate from planar have a higher surface-area-to-volume ratio. Consequently, features that rise above the plane will be etched faster until they are smoothed to the level of the plane.

The transition temperature of ~270 °C between AlF_3 growth and Al_2O_3 etching can also be identified by observing the surface roughness after 100 reaction cycles at different temperatures. Figure 12(b) shows the measured roughness of the resulting substrate after 100 R-ALE cycles with a pulse sequence of (1, 0, 1, 0) using pressures of HF = 320 mTorr and TMA = 160 mTorr. The surface roughness of the initial Al_2O_3 ALD film was again 6.26 Å. The surface roughness increases at temperatures below 270 °C where AlF_3 growth occurs with sequential HF and TMA exposures.[26] The surface roughness decreases at temperatures above 270 °C where Al_2O_3 etching occurs with sequential HF and TMA exposures.

C. Etching in high aspect ratio structures

Si wafers with an array of high aspect ratio structures were obtained from TEL Technology Center, America, LLC, Albany, NY for R-ALE experiments. The surface of these structures was coated with an SiO_2 film thickness of ~24 nm. Al_2O_3 ALD films were then deposited on these structures using TMA and H_2O to produce an Al_2O_3 film thickness of ~28 nm. Subsequently, etching experiments using timing sequences of (1, 0, 1, 0), (1, 1, 1, 1), and (1, 30, 1, 30) were performed on separate samples at 300 °C. The partial pressures during these experiments were 320 and 160 mTorr for HF and TMA, respectively. Following etching, the samples were sent to TEL Technology Center, America, LLC in Albany, NY, for cross-sectional SEM analysis of vias with an aspect ratio of 7:1 before and after Al_2O_3 R-ALE.

Figure 13 displays the initial Al_2O_3 ALD films along with etching results after 130 cycles of etching with the various

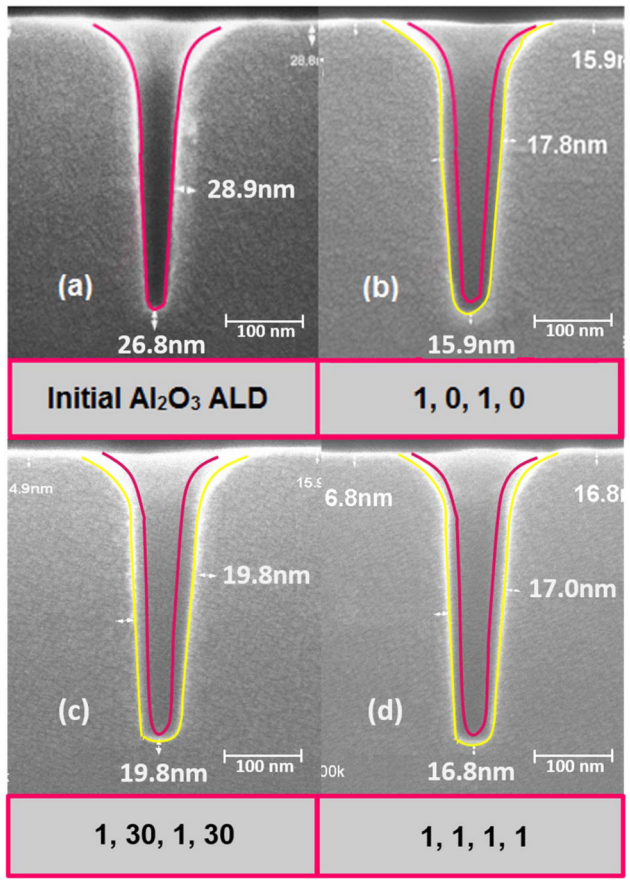

FIG. 13. Cross-sectional SEM analysis of vias in patterned wafer: (a) via with the Al_2O_3 ALD film; (b) via after 130 cycles of Al_2O_3 R-ALE at 300 °C with timing sequence of (1, 0, 1, 0); (c) via after 130 cycles of Al_2O_3 ALE at 300 °C with timing sequence of (1, 30, 1, 30); (d) via after 130 cycles of Al_2O_3 etching at 300 °C with timing sequence of (1, 1, 1, 1). The reactant pressures were HF = 320 mTorr and TMA = 160 mTorr.

timing sequences. The conformality of the Al_2O_3 ALD films with a thickness of ~28 nm was confirmed by the SEM image in Fig. 13(a). The variation in the film thickness from the left to right side of the via is a result of cross sectioning the via slightly asymmetrically. Figure 13(b) displays a via after 130 cycles of Al_2O_3 R-ALE using the timing sequence of (1, 0, 1, 0). This image shows conformal etching that reaches into the deepest section of the via at an average etch rate of 0.9 Å/cycle.

In comparison, Fig. 13(c) displays the image of a via after 130 cycles of Al_2O_3 ALE using a timing sequence of (1, 30, 1, 30). In similarity with the R-ALE results shown in Fig. 12(b), Al_2O_3 ALE also results in uniform etching. However, the etch rate is reduced to 0.6 Å/cycle. The Al_2O_3 ALE cycle time is also 31 times longer than the Al_2O_3 R-ALE cycle time. One advantage that Al_2O_3 ALE displays compared with Al_2O_3 R-ALE is the profile at the bottom of the via. Al_2O_3 ALE shows a slightly flatter profile at the bottom of the via than Al_2O_3 R-ALE. Figure 13(d) shows the image of a via after 130 cycles of Al_2O_3 etching using a timing sequence of (1, 1, 1, 1). This timing sequence allows for a slight time separation between the HF and TMA reactants. With this 1 s purge time, the etch rate is higher at 0.8 Å/cycle and there is still a flat profile at the bottom of the via.

D. Etch rate with precursor overlap

The results in this paper on Al_2O_3 R-ALE have demonstrated that Al_2O_3 etching is possible with no purging using the timing sequence of (1, 0, 1, 0). The question remains whether overlap between the HF and TMA exposures will lead to AlF_3 growth by CVD or Al_2O_3 etching by CVE. To answer this question, experiments directly overlapped the TMA and HF exposures on an initial Al_2O_3 ALD film at 300 °C. The QCM results for this combined TMA and HF exposure are shown in Fig. 14(a). The individual TMA and HF partial pressures were 160 and 320 mTorr, respectively. The valves were open for 1 s. Figure 14(a) displays a dramatic mass increase consistent with AlF_3 CVD.

After approximately 28 s in Fig. 14(a), the AlF_3 CVD film was exposed to TMA only. Figure 14(a) shows that the TMA exposure was able to etch the entire AlF_3 CVD film and return the mass to the original mass of the Al_2O_3 ALD film. The TMA exposure was defined by a TMA partial pressure of 160 mTorr for 3 s. These results suggest that any AlF_3 CVD film that results from TMA and HF overlap can be easily removed by subsequent TMA exposures.[26]

Additional QCM experiments were performed by varying the overlap between sequential HF and TMA exposures while keeping the total cycle time fixed at 2 s. The HF and TMA exposures during these overlap experiments produced individual pressure transients of 320 and 160 mTorr, respectively. Partial overlap between the precursors in time for 0.5 s is illustrated by Fig. 1(b) for the timing sequence of (1, −0.5, 1, 0.5). Complete overlap between the precursors in time for 1.0 s is illustrated by Fig. 1(c) for the timing sequence of (1, −1, 1, 1).

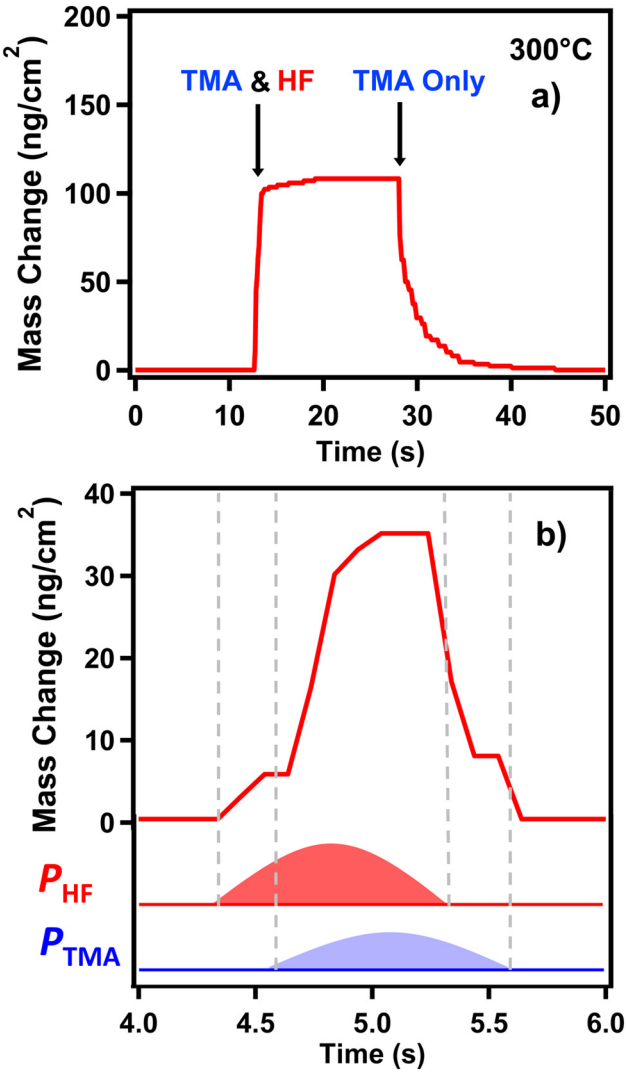

FIG. 14. (a) Mass change resulting from the overlap of HF and TMA exposures for 1 s, and then a subsequent TMA exposure for 3 s. (b) Mass change during one Al_2O_3 R-ALE cycle during a timing sequence of (1, −0.75, 1, 0.75). The reactant pressures were HF = 320 mTorr and TMA = 160 mTorr.

Figure 15 presents the MCPC versus precursor overlap time for 50 cycles of etching with various timing sequences. The degree of precursor exposure overlap was adjusted between 0 and 1 s by 0.25 s increments and the total cycle time was maintained at 2 s by varying the purge time. The timing sequences were (1, 0, 1, 0) with no precursor overlap; (1, −0.25, 1, 0.25) with a precursor overlap of 0.25 s; (1, −0.5, 1, 0.5) with a precursor overlap of 0.5 s; (1, −0.75, 1, 0.75) with a precursor overlap of 0.75 s; and (1, −1, 1, 1) with complete 1 s precursor overlap.

Figure 15 shows that the largest negative MCPC of −32.1 ng/(cm^2 cycle) occurs with no precursor overlap. Increasing the precursor overlap leads to progressively less Al_2O_3 etching. The MCPC decreases to −20.0 and −13.0 ng/(cm^2 cycle) at overlap times of 0.25 and 0.50 s, respectively. There is no evidence of larger mass losses that might have been expected for Al_2O_3 CVE. Likewise, there is no evidence for mass gains that may have been anticipated for AlF_3 CVD.

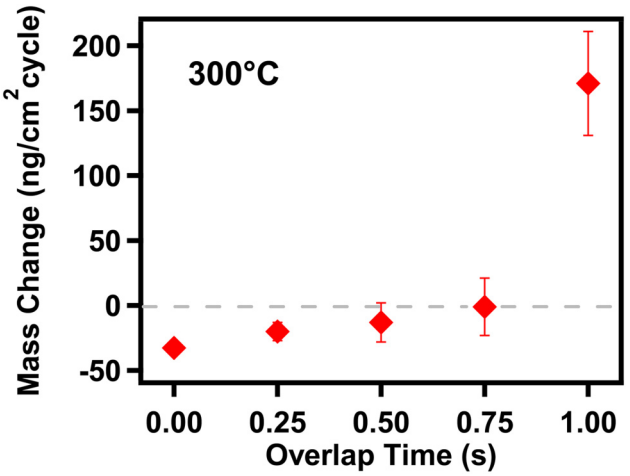

FIG. 15. Etch rate vs overlap time between precursor pulses using sequential exposures of HF and TMA at 300 °C. The timing sequences were (1, 0, 1, 0), (1, −0.25, 1, 0.25), (1, −0.5, 1, 0.5), (1, −0.75, 1, 0.75), and (1, −1, 1, 1) for overlap times of 0, 0.25, 0.5, 0.75, and 1.0 s, respectively, with a total cycle time of 2.0 s. The reactant pressures were HF = 320 mTorr and TMA = 160 mTorr.

The MCPC decreases to a negligible value of −0.99 ng/(cm^2 cycle) at an overlap time of 0.75 s. Under these conditions, AlF_3 growth and Al_2O_3 etching are nearly balanced.

For the direct overlap of the TMA and HF exposures for the full 1 s, Fig. 15 reveals that there is a dramatic positive MCPC of +171 ng/(cm^2 cycle). This positive MCPC is consistent with the growth of an AlF_3 CVD film as expected from the results in Fig. 14(a). In this case, there is no removal of the AlF_3 CVD film because the TMA and HF are directly overlapped for the full 1 s. There is no extra TMA exposure remaining after the overlap to etch the AlF_3 film.

The QCM results were then analyzed in time during the overlap of the TMA and HF exposures. Figure 14(b) displays the time-dependent results for the timing sequence of (1, −0.75, 1, 0.75). There is a mass increase during the overlap of the TMA and HF exposures. However, the entire mass increase is subsequently removed by the TMA exposure remaining after the precursor overlap. The TMA exposure is able to etch the AlF_3 CVD film that was deposited during the overlap of the TMA and HF exposures.[26]

Purgeless Al_2O_3 R-ALE can be understood in terms of the schematic in Fig. 16. HF exposures fluorinate the Al_2O_3 surface. In the absence of a purge, overlap between the HF and TMA exposures produce AlF_3 CVD. However, the subsequent TMA exposure can spontaneously etch the AlF_3 film that results from either AlF_3 CVD or the fluorination of the Al_2O_3 surface. The ability of TMA to etch the AlF_3 CVD film removes the consequence of precursor overlap during purgeless R-ALE.

R-ALE should be possible with other thermal ALE systems where the two precursors in the process could yield either ALE or ALD. This condition should be common for thermal ALE systems based on fluorination and ligand-exchange reactions. For example, Al_2O_3 R-ALE should also be possible with $Sn(acac)_2$ and HF as the precursors because $Sn(acac)_2$ and HF can either produce SnF_2 ALD or Al_2O_3 ALE.[12,14] The $Sn(acac)_2$ metal precursor can either adsorb to produce a surface intermediate or undergo ligand-exchange with the AlF_3 surface layer to etch the substrate.[12,14] HF can then

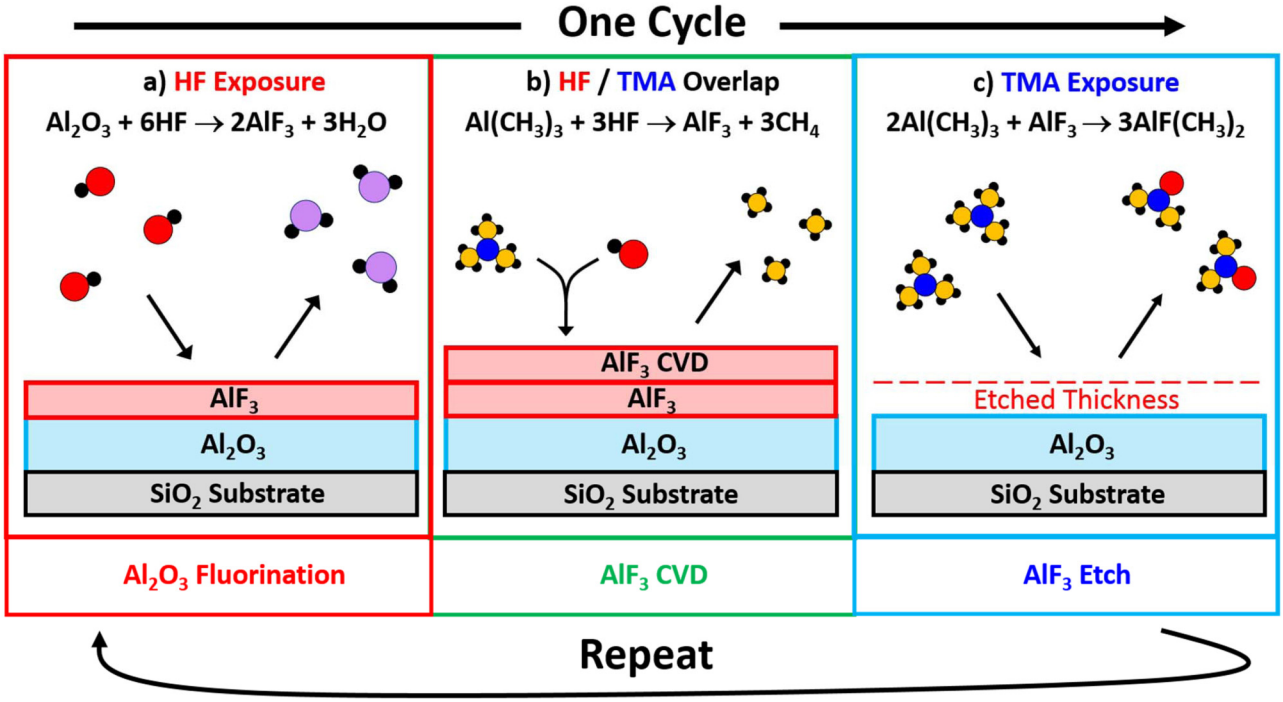

FIG. 16. Schematic showing one cycle of Al_2O_3 R-ALE composed of (a) an HF exposure that fluorinates Al_2O_3 to produce an AlF_3 surface layer; (b) the overlap between the HF and TMA exposures that can lead to AlF_3 CVD; and (c) the subsequent TMA exposure that can remove the AlF_3 CVD film and underlying AlF_3 surface layer.

either fluorinate the Al_2O_3 substrate to form an AlF_3 surface layer during ALE or fluorinate the surface intermediate to produce SnF_2 ALD.[12,14]

IV. CONCLUSIONS

The R-ALE of Al_2O_3 was demonstrated between ~270 and 325 °C using sequential exposures of HF and TMA with no purging. *In situ* QCM measurements observed linear mass loss versus time during the rapid etching process using precursor pulse times of 1 s. The mass changes were consistent during each HF and TMA exposure with averages of $\Delta M_{HF} = 28.6$ ng/(cm^2 cycle) and $\Delta M_{TMA} = -60.7$ ng/(cm^2 cycle) at 300 °C with a pulse sequence of (1, 0, 1, 0) using partial pressures of HF = 320 mTorr and TMA = 160 mTorr. The mass change per cycle was MCPC = −32.1 ng/(cm^2 cycle). This MCPC corresponds with an etch rate of 0.99 Å/cycle. Lower MCPC values were observed at lower partial pressures of HF and TMA. Additional QCM studies demonstrated that the HF and TMA exposures were self-limiting versus precursor partial pressure during Al_2O_3 R-ALE.

Al_2O_3 R-ALE using a timing sequence of (1, 0, 1, 0) was compared with Al_2O_3 ALE using a timing sequence of (1, 30, 2, 30). At the same reactant exposures for HF and TMA, the MCPC values were nearly equivalent for Al_2O_3 R-ALE and Al_2O_3 ALE. However, the etch rate was 36.5 times faster for R-ALE because of its shorter cycle time. In addition, Al_2O_3 R-ALE smoothed the initial Al_2O_3 film versus number of R-ALE cycles. The Al_2O_3 film roughness was reduced from an initial roughness of 6.26 to 3.65 Å after 100 R-ALE cycles at 300 °C. The Al_2O_3 etch rate was also temperature dependent and varied from −0.02 Å/cycle at 270 °C to 1.12 Å/cycle at 325 °C. Temperatures below 270 °C led to AlF_3 ALD. The etch rate and the surface roughness both revealed a transition temperature between AlF_3 ALD and Al_2O_3 ALE at ~270 °C.

Cross-sectional SEM analysis was performed after Al_2O_3 R-ALE and Al_2O_3 ALE on high aspect ratio structures with aspect ratios of 7:1. The cross-sectional SEM images revealed that the etching was isotropic and conformal for both Al_2O_3 R-ALE with a timing sequence of (1, 0, 1, 0) and Al_2O_3 ALE with a timing sequence of (1, 30, 1, 30). Additional experiments measured the etch rate versus the overlap of the precursor exposures in time. The etch rate was observed to decrease progressively versus overlap time. Negligible etching was observed with nearly complete overlap between the HF and TMA exposures. However, complete precursor overlap produced significant AlF_3 CVD. This AlF_3 CVD could be easily removed by a subsequent TMA exposure. These results suggest a model for Al_2O_3 R-ALE where any possible AlF_3 CVD during precursor overlap is spontaneously etched by the subsequent TMA exposure.

R-ALE is a significant development in the field of atomic layer processing. One criticism of both ALE and ALD is their long cycle times and slow etching or growth. The elimination of the purge step during thermal Al_2O_3 R-ALE produces higher etching per cycle and dramatically increases the etching per time. R-ALE may be extended to other thermal ALE processes that have utilized long purge times to avoid possible CVE or CVD. The rapid etching rates during R-ALE are expected to facilitate many future R-ALE applications.

ACKNOWLEDGMENTS

This research was funded by Tokyo Electron Limited. Additional support was provided by the National Science Foundation through Grant No. CHE-1609554. The authors would like to thank Jozef Brcka at TEL Technology Center, America, LLC, Austin, TX for useful discussions. The authors also thank Huaxing Sun for the XPS elemental analysis and the TEL Technology Center, America, LLC in Albany, NY, for SEM imaging. The authors acknowledge Jasmine Wallas and Jaclyn Sprenger for XRR and XRD measurements.

[1]K. J. Kanarik, T. Lill, E. A. Hudson, S. Sriraman, S. Tan, J. Marks, V. Vahedi, and R. A. Gottscho, J. Vac. Sci. Technol. A **33**, 020802 (2015).
[2]S. M. George, Chem. Rev. **110**, 111 (2010).
[3]S. M. George and Y. Lee, ACS Nano **10**, 4889 (2016).
[4]S. D. Athavale and D. J. Economou, J. Vac. Sci. Technol. B **14**, 3702 (1996).
[5]S. D. Park, D. H. Lee, and G. Y. Yeom, Electrochem. Solid State Lett. **8**, C106 (2005).
[6]T. Matsuura, T. Sugiyama, and J. Murota, Surf. Sci. **402**, 202 (1998).
[7]W. S. Lim, S. D. Park, B. J. Park, and G. Y. Yeom, Surf. Coat. Technol. **202**, 5701 (2008).
[8]D. Metzler, R. L. Bruce, S. Engelmann, E. A. Joseph, and G. S. Oehrlein, J. Vac. Sci. Technol. A **32**, 020603 (2014).
[9]J. B. Park, W. S. Lim, B. J. Park, I. H. Park, Y. W. Kim, and G. Y. Yeom, J. Phys. D: Appl. Phys. **42**, 055202 (2009).
[10]Y. Y. Kim, W. S. Lim, J. B. Park, and G. Y. Yeom, J. Electrochem. Soc. **158**, D710 (2011).
[11]J. W. DuMont and S. M. George, J. Chem. Phys. **146**, 052819 (2017).
[12]Y. Lee, J. W. DuMont, and S. M. George, Chem. Mater. **27**, 3648 (2015).
[13]Y. Lee, J. W. DuMont, and S. M. George, Chem. Mater. **28**, 2994 (2016).
[14]Y. Lee and S. M. George, ACS Nano **9**, 2061 (2015).
[15]J. Hennessy, C. S. Moore, K. Balasubramanian, A. D. Jewell, K. France, and S. Nikzad, J. Vac. Sci. Technol. A **35**, 041512 (2017).
[16]Y. Lee, J. W. DuMont, and S. M. George, J. Phys. Chem. C **119**, 25385 (2015).
[17]Y. Lee, J. W. DuMont, and S. M. George, ESC J. Solid State Sci. Technol. **4**, N5013 (2015).
[18]J. W. DuMont, A. E. Marquardt, A. M. Cano, and S. M. George, ACS Appl. Mater. Interfaces **9**, 10296 (2017).
[19]D. R. Zywotko and S. M. George, Chem. Mater. **29**, 1183 (2017).
[20]N. R. Johnson, H. Sun, K. Sharma, and S. M. George, J. Vac. Sci. Technol. A **34**, 050603 (2016).
[21]Y. Lee and S. M. George, Chem. Mater. **29**, 8202 (2017).
[22]N. R. Johnson and S. M. George, ACS Appl. Mater. Interfaces **9**, 34435 (2017).
[23]T. Faraz, F. Roozeboom, H. C. M. Knoops, and W. M. M. Kessels, ECS J. Solid State Sci. Technol. **4**, N5023 (2015).
[24]M. D. Groner, F. H. Fabreguette, J. W. Elam, and S. M. George, Chem. Mater. **16**, 639 (2004).
[25]J. W. Elam, M. D. Groner, and S. M. George, Rev. Sci. Instrum. **73**, 2981 (2002).
[26]Y. Lee, J. W. DuMont, A. S. Cavanagh, and S. M. George, J. Phys. Chem. C **119**, 14185 (2015).
[27]M. N. Rocklein and S. M. George, Anal. Chem. **75**, 4975 (2003).
[28]V. Tsionsky, L. Daikhin, M. Urbakh, and E. Gileadi, Langmuir **11**, 674 (1995).
[29]R. Matero, A. Rahtu, M. Ritala, M. Leskela, and T. Sajavaara, Thin Solid Films **368**, 1 (2000).
[30]R. L. Puurunen, J. Appl. Phys. **97**, 121301 (2005).
[31]*HSC Chemistry*, HSC Chemistry 5.1, Outokumpu Research Oy, Pori, Finland.
[32]B. E. Deal and A. S. Grove, J. Appl. Phys. **36**, 3770 (1965).
[33]N. B. Pilling and R. E. Bedworth, J. Inst. Met. **29**, 529 (1923).
[34]R. L. Puurunen, M. Lindblad, A. Root, and A. O. I. Krause, Phys. Chem. Chem. Phys. **3**, 1093 (2001).